

TOP QUARKS*†

J.H. KÜHN

Institut für Theoretische Teilchenphysik
Universität Karlsruhe
D-76128 Karlsruhe, Germany

(Received March 27, 1995)

Recent theoretical results on the production and decay of top quarks are presented. The implications of the new experimental results from the TEVATRON are briefly discussed. Predictions for the top quark decay rate and distributions are described, including the influence of QCD and electroweak radiative corrections. Top production at an e^+e^- collider is discussed with emphasis towards the threshold region. The polarization of top quarks in the threshold region is calculated with techniques based on Green's functions for S and P waves.

PACS numbers: 14.65.Ha

1. Introduction

The ever-increasing energies of electron positron colliders from PETRA, PEP, and TRISTAN up to LEP as well as those of the hadron colliders $Spp\bar{p}S$ and TEVATRON have led for a long time only to a steady increase of the lower bound of the top quark mass. The direct limits from LEP of about 45 GeV and the indirect limit from the absence of $W \rightarrow t + b$ as inferred from the W decay rate (62 GeV) were derived in a fairly model-independent way. With increasing luminosity at the TEVATRON the limit had increased steadily until the spring of 1994 when first evidence for the top quark was presented by the CDF collaboration [1]. Finally, after collecting a data sample corresponding to 67 pb^{-1} , the top quark has been observed by both collaborations CDF [2] as well as DØ [3] with a mass of about 176 GeV and 199 GeV respectively.

* Presented at the Cracow Epiphany Conference on Heavy Quarks, held in honour of the 60th birthday of Kacper Zalewski, Kraków, Poland, January 5–6, 1995.

† Work supported by BMFT contract 0056KA93P.

These results are nicely consistent with precision measurements of electroweak parameters which exploit the quadratic top mass dependence [4] of the ρ -parameter, resulting in [5] $m_t = 178 \pm 11 \pm 19$ GeV where the second error originates from the variation of the Higgs mass between 60 GeV and 1 TeV with a central value at 300 GeV.

The discovery of the top quark has completed the fermionic spectrum of the Standard Model. The precise determination of its mass will provide important input for all calculations, leaving the Higgs mass as only free parameter which could then be inferred from precise measurements planned at LEP in the near future. The study of the top quark and its decay modes will thus constitute an important part of the physics program at the TEVATRON, the LHC, and the future linear collider.

After the discovery of the top quark in hadronic collisions and the subsequent exploratory studies, electron-positron experiments will serve to determine its mass with high precision, and to explore its gauge coupling to the W and Z bosons. The Yukawa coupling to the Higgs boson which drives the large top mass should be measured and might provide important information on the mechanism of fermion mass generation. A variety of novel QCD studies is at hand as a consequence of its rapid weak decay which intercepts the hadronization process. Close to threshold one may explore the QCD potential, and eventually the Yukawa potential induced by Higgs exchange. Decay modes of the top which are predicted in extensions of the Standard Model (SM) could be searched, for example decays into a charged Higgs boson plus a bottom quark or into the supersymmetric partner of the top plus a photino, or one may even search for FCNC decays. Also new couplings can be explored with sufficient statistics, for example an anomalous magnetic moment or CP violating coupling at the $Zt\bar{t}$ or the $Wt\bar{t}$ vertex.

After a brief discussion of the recent discovery of the top quark Section 2 of this review will be concerned with the present status of the calculations for the decay of top quarks. In a first step the total decay rates, QCD and electroweak corrections will be treated and potential deviations in extensions of the SM discussed. Calculations of the spectrum of W s and leptons from top decays will be summarized. The prediction for $t\bar{t}$ production in e^+e^- annihilation is summarized in Section 3. Emphasis is put on the threshold region and the remnants of toponium. This includes a discussion of the total cross section and of momentum distributions, of theoretical ambiguities in the top mass determination, and of relativistic corrections. Recent results concerning the polarization of top quarks in the threshold region will be treated in Section 4.

2. Mass, decay rate and distributions

2.1. Top quark mass

After collecting a large amount of data in $p\bar{p}$ collisions at an energy of 1.8 TeV, corresponding to 67 pb^{-1} for the CDF experiment and 50 pb^{-1} for DØ, both collaborations have reported the observation of the top quark, tagged in $t\bar{t}$ events where one quark decays semileptonically, the other hadronically or also semileptonically. With a production cross section of $6.8^{+3.6}_{-2.4} \text{ pb}$ as measured by CDF and $6.4 \pm 2.2 \text{ pb}$ from DØ theory and experiment are in fair agreement for a mass around 180 GeV as demonstrated in Fig. 1 (taken from [3]).

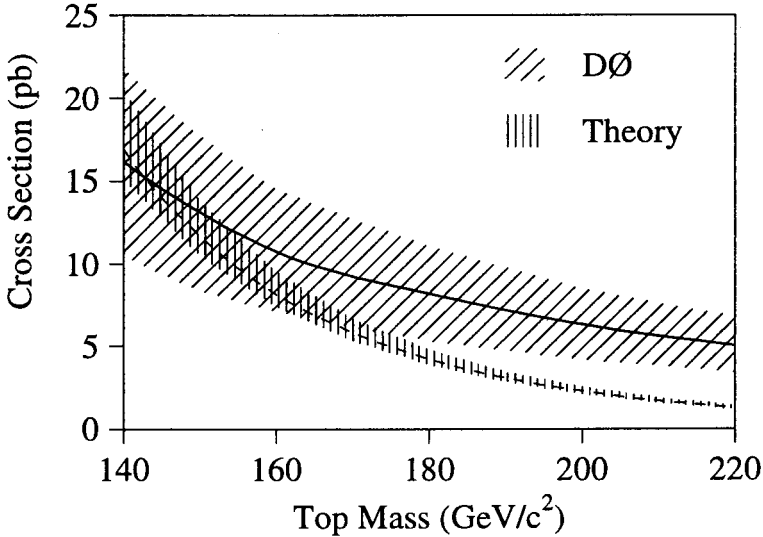


Fig. 1. DØ measured $t\bar{t}$ production cross section (solid line with one standard deviation error band) as a function of assumed top quark mass. Also shown is the theoretical cross section curve (dashed line).

On the other hand the sample of reconstructed top events leads to a mass of $m_t = 176 \pm 8 \pm 10 \text{ GeV}$ at CDF (Fig. 2) and $m_t = 199^{+19}_{-21} \pm 22 \text{ GeV}$ at DØ nicely consistent with the cross section measurements.

This important result not only provides the final quark required for consistency of the SM. The agreement of the mass measurements with the predictions based on electroweak radiative corrections of $178 \pm 11 \pm 19 \text{ GeV}$ [5] confirms the importance of quantum corrections in the electroweak theory. A reduction of the uncertainty in the mass determination down to

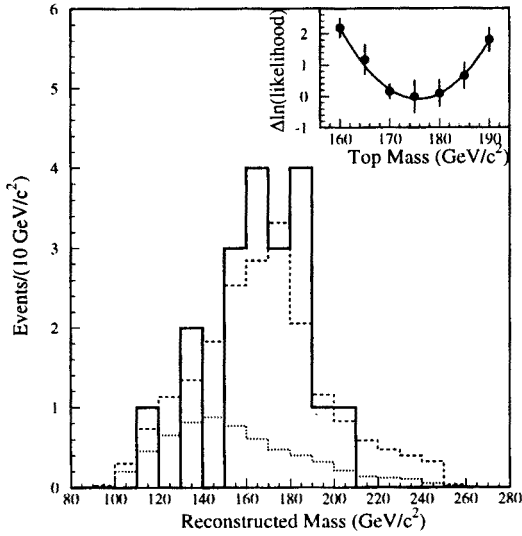


Fig. 2. Reconstructed mass distribution for the b -tagged $W + \geq 4$ -jet events (solid). Also shown are the background shape (dotted) and the sum of background plus $t\bar{t}$ Monte Carlo for $M_{\text{top}} = 175 \text{ GeV}/c^2$ (dashed), with the background constrained to the calculated value, $6.9^{+2.5}_{-1.9}$ events. The inset shows the likelihood fit used to determine the top mass.

about $\pm 1 \text{ GeV}$ as expected from experiments at a linear electron positron collider would allow to fully exploit the precision expected in electroweak observables in the near future (Fig. 3).

However, also a modest $\delta m_t = \pm 5 \text{ GeV}$ which could be achieved at the LHC would lead to important restrictions on the mass of the Higgs boson in the Standard Model.

The discovery has immediate implications for top decays: If the experimentally measured and the calculated cross section are in good agreement, then the decay mode $t \rightarrow b + W$ must be dominant and any more exotic channel like $t \rightarrow bH$ or decays envisaged in SUSY models like $t \rightarrow \tilde{t}\tilde{\gamma}$ can only appear as small admixtures. This justifies to study the top decay mode $t \rightarrow bW$, including all refinements of QCD and electroweak corrections.

2.2. Top decays

Top quark physics is to a large extent dictated by the large decay rate (Fig. 4), which quickly reaches its asymptotic form

$$\Gamma(t \rightarrow b + W^+) \rightarrow 175 \text{ MeV} \cdot \left(\frac{m_t}{m_W} \right)^3. \quad (1)$$

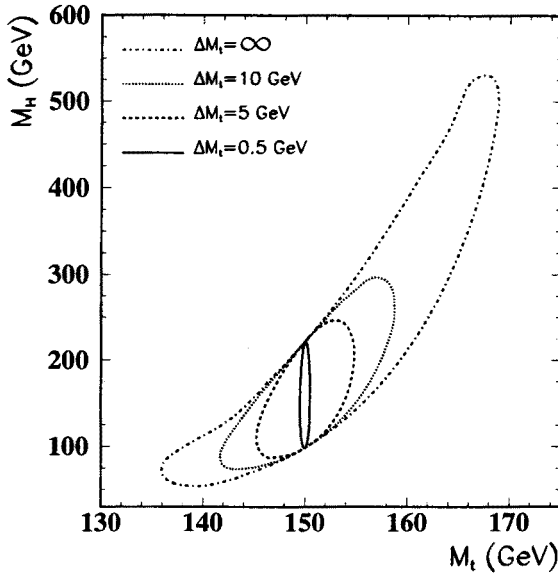


Fig. 3. Constraints on the Higgs mass for a central value of 150 GeV from final data of LEP I, the direct W -mass measurements and the left-right e^+e^- polarization asymmetry, if the mass is determined externally with large or small error [5].

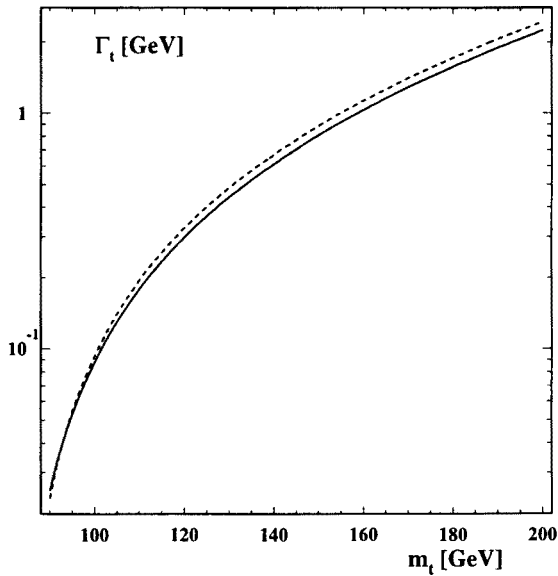


Fig. 4. Solid line: The width of the top quark in the SM, including QCD and electroweak corrections and the finite W width. Dashed line: Born and narrow width approximation.

Three steps in the increase of the decay rate affect the qualitative behavior of top mesons [6]:

- i) Once m_t is above 70 GeV the hyperfine splitting between T and T^* cannot be resolved anymore:

$$m_{T^*} - m_T \propto 1/m_t < 1 \text{ MeV} \ll \Gamma_t.$$

The angular distribution of all decay products follow the predictions derived for a spin $1/2$ t -quark and may serve to analyze the top spin.

- ii) Above 100 GeV the width exceeds 100 MeV, the characteristic scale for the formation of top mesons. No T or T^* mesons can be formed.
- iii) Toponium states are severely affected once m_t is above 130 GeV, leading to a toponium width $2\Gamma_t \geq 0.88 \text{ GeV}$ comparable to the $1S$ - $2S$ mass difference. A complicated interplay between binding forces and the rapid decay is predicted. Hence, for the actual value of $m_t \approx 180 \text{ GeV}$ energy and angular distributions of all decay products can be described to a good approximation by those resulting of the decay of "free" spin $1/2$ quarks.

These quantitative considerations are supplemented by precise calculations including QCD and electroweak corrections to the decay rate and the spectra. A reduction of Γ_t by a relative amount $\delta_{\text{QCD}}^{(1)}$ of about 8% is induced by QCD [7, 8]. QCD corrections including the effects from the nonvanishing Γ_W and m_b are also contained in these papers. They are conventionally cast into the form:

$$\Gamma = \Gamma_{\text{Born}} \left(1 - \frac{2}{3} \frac{\alpha_s}{\pi} f(m_t, m_W, m_b, \Gamma_W) \right). \quad (2)$$

In the narrow width approximation and for vanishing bottom mass a particularly simple formula has been derived for the correction function f :

$$f = [\pi^2 + 2Li_2(y) - 2Li_2(1-y)] + \frac{4y(1-y-2y^2)\ln y + 2(1-y)^2(5+4y)\ln(1-y) - (1-y)(5+9y-6y^2)}{2(1-y)^2(1+2y)}, \quad (3)$$

where $y = m_W^2/m_t^2$. This approximation describes the exact correction function to better than 1% for m_t above 160 GeV. In fact, even the asymptotic result $f(0) = \frac{2}{3}\pi^2 - \frac{5}{2} \approx 4.08$ provides an adequate approximation which is valid to about 10% accuracy. In general $\mu^2 \approx m_t^2$ is adopted for the characteristic scale of $\alpha_s(\mu^2)$. Recently, however, arguments based on partial calculations have been given [9] that the effective scale should be

reduced significantly down to $\mu = 0.28m_t$ which would lead to a significant decrease of the rate.

Potentially large electroweak corrections could be expected from the enhanced Yukawa couplings, providing terms $\propto m_t^2/m_W^2$. However, as shown in [10] large accidental cancellations among these leading terms render the weak corrections fairly small. This result has been confirmed and strengthened by the full calculation performed in [11, 12]. These electroweak corrections increase the rate by a relative amount δ_{ew} of about 1.5%.

The finite width of the W leads to a reduction δ_{Γ_W} of about the same magnitude [8]. The individual corrections and the overall predictions are displayed in Table I for a few characteristic masses.

Several sources of theoretical uncertainties remain. Not yet calculated $\mathcal{O}(\alpha_s^2)$ -terms can be estimated to contribute about 1-2%, the influence of the uncertainty in m_t (estimated to .5 GeV) will induce another 1%. With an estimated experimental resolution of about 5 to 10% at best at a future linear collider, these theoretical uncertainties will not pose a serious problem in the foreseeable future. At a hadron collider no measurement of the decay rate can be performed.

TABLE I

Top width as a function of top mass and the comparison of the different approximations.

m_t (GeV)	$\alpha_s(m_t)$	$\Gamma_{nw}^{\text{Born}}$ (GeV)	$\delta_{\Gamma_w}^{(0)}$ (%)	$\delta_{\text{QCD}}^{(1)}$ (%)	δ_{ew} (%)	Γ_t (GeV)
170.0	.108	1.405	-1.52	-8.49	1.67	1.287
180.0	.107	1.714	-1.45	-8.48	1.70	1.572
190.0	.106	2.059	-1.39	-8.47	1.73	1.890

An important issue will be the search for new decay modes expected in extensions of the Standard Model.

The impact of the two Higgs doublet model (THDM) on radiative corrections to $t \rightarrow W + b$ is fairly small [13] and similar results are expected for the minimal supersymmetric SM (MSSM). However, new decay modes with sizable rates are possible for appropriate mass combinations, for example $t \rightarrow b + H^+$ or $t \rightarrow \tilde{t} + \tilde{\gamma}$. Large branching ratios are conceivable in the most general THDM for the decay into the charged Higgs boson which may even dominate if the ratio between the two vacuum expectation values $v_1/v_2 = \tan\beta$ is chosen sufficiently small, corresponding to an enhanced tbH Yukawa coupling above its "natural" value of $m_t\sqrt{\sqrt{2}G_F}$. However, this choice is theoretically unattractive and with the top quark discovery at the TEVATRON already excluded. For the "natural" range of $\tan\beta$ between 1 and m_t/m_b one predicts branching ratios from a few up to 25%.

These considerations can be made more quantitative in the context of the MSSM [14].

FCNC decays into a charmed quark plus a gluon, photon, Z or Higgs boson are entirely negligible in the context of the SM, with branching ratios of 10^{-7} down to 10^{-12} [15]. The perspectives are more favorable if conventional quarks mix with new quarks which might exist in $SU(2)$ representations different from $I = 1/2$. Typical examples are quarks in vector representations, isosinglet quarks, or mirror quarks.

2.3. Distributions

The lowest-order prediction for the energy and angular distribution of leptons from a polarized top quark in the narrow width approximation and with $m_b = 0$ is extremely simple and factorizes into an energy and an angular dependent term

$$\frac{dN}{d\cos\theta dx} \propto x(1-x)(1+\cos\theta). \quad (4)$$

The lepton angular distribution is therefore an ideal tool to analyze the polarization of top quarks which is induced either through longitudinal beam polarization or — naturally — through γZ interference. QCD corrections, including mass effects and the nonvanishing W width, are available in the literature [16]. Their impact on the lepton spectrum is quite important, the angular dependence, however, is hardly affected. Charged lepton angular distributions are therefore an ideal tool to determine the spin of top quarks. Neutrino distributions, on the other hand, are particularly sensitive towards small admixtures of righthanded currents in the tbW coupling [17]. Predictions for the W energy distribution are also available [18, 19].

3. Production in e^+e^- collisions

3.1. Far above threshold

The cross section for $e^+e^- \rightarrow t\bar{t}$ is fairly large throughout. It starts with a step-function-like increase to $R \approx 0.7$ at threshold as a consequence of the Coulomb enhancement $\propto 1/v$ and increases to a value of $R \approx 2$ for energies above $2m_t + 100$ GeV (Fig. 5). Electroweak radiative corrections to top production at threshold and in the continuum have been calculated in [20, 21]. Relative to the G_F parametrized Born approximation they decrease the cross section by -6% to -9%, if m_t is varied between 100 and 200 GeV, m_H between 40 and 1000 GeV and E_{cm} fixed to 500 GeV. The influence of Higgs exchange on the threshold behavior has been discussed in more detail in [22].

The production cross section for $t\bar{t}$ has to be contrasted with the potential backgrounds $f\bar{f}$, WW and ZZ . Detailed simulations demonstrate [23] that a signal-to-noise ratio of 10 can be achieved with an efficiency of 30%. The top mass can be determined with an estimated uncertainty of about 0.5 GeV.

The large top decay rate allows for a variety of novel QCD studies. The rapid decay intercepts the evolution of the string of soft hadrons between t and \bar{t} [24]. Perturbative soft gluon radiation is similarly affected and cut off for particular kinematic configurations [25]. This effect is particularly pronounced for e^+e^- energies in the TeV range.

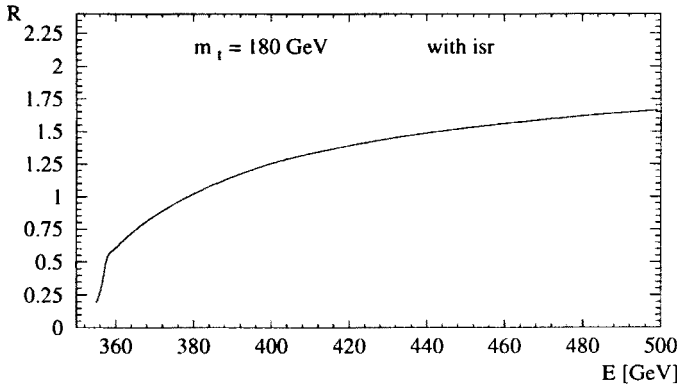


Fig. 5. Cross section for $t\bar{t}$ production, including resonances, QCD corrections and initial state radiation in units of σ_{point} .

Yukawa couplings: The determination of the $t\bar{t}H$ coupling constitutes one of the central aims of top quark studies at a linear collider. Apart from the influence of Higgs exchange in the threshold region two reactions have been suggested which are sensitive to the Yukawa coupling: for small Higgs mass the radiation of a real Higgs boson [26]

$$e^+e^- \rightarrow t\bar{t}H, \quad (5)$$

for a heavy Higgs boson the reaction [27]

$$e^+e^- \rightarrow t\bar{t}Z \quad (6)$$

which receives important contributions from an intermediate Higgs boson. Given favorable mass assignments these reactions might be experimentally accessible.

3.2. Cross section in the threshold region

A lot of effort has been invested during the past years in the theoretical study of the total cross section and of momentum distributions in the threshold region. For a stable top quark one would expect a series of narrow toponium bound states. As a consequence of the large decay rate of the top quark only remnants of these resonances can be observed which merge into a fairly smooth cross section. Nevertheless a number of important topics can be investigated in this region: *i)* The top mass can be determined with high precision. *ii)* The QCD interquark potential can be probed down to very small distances. *iii)* The production of a large number of polarized top quarks practically at rest allows the study of form factors and of conventional and potentially new decay modes under simple kinematic conditions. *iv)* Under favorable circumstances, namely a light Higgs and a heavy top, one may become sensitive toward the Yukawa coupling.

As stated before, one faces a series of many overlapping resonances, once m_t lies above 120 GeV. A convenient technique to perform this summation was proposed in [28]. The sum over individual Breit Wigner resonances multiplied by the wave function at the origin is easily transformed into the imaginary part of the Green's function.

$$\begin{aligned} \sum_n |\psi_n(0)|^2 \frac{\Gamma_t}{(E_n - E)^2 + \Gamma_t^2} &= \sum_n \text{Im} \frac{\psi_n(0)\psi_n^*(0)}{E_n - E - i\Gamma_t} \\ &= \text{Im} G(0, 0, E + i\Gamma). \end{aligned} \quad (7)$$

The Green's function can be obtained as the solution of the inhomogeneous Schrödinger equation with a δ function like source term, located at $\vec{x} = 0$ and with an oscillatory time dependence $\exp(-iEt)$ that has been factored out. G can be calculated analytically for a pure Coulomb potential and numerically [29] for the more realistic QCD potential, whose short distance behavior includes the proper running of α_s .

The height of the peak cross section, the exact location of the threshold and the relative momentum of the top quarks (see below) depend sensitively on the actual value of $\Lambda_{\overline{MS}}$ or α_s (Fig. 6). Resonance and QCD corrected continuum cross section join smoothly [30].

3.3. Momentum distributions

The momentum distribution of top quarks from an individual resonance can be calculated from the Fourier transform of the wave functions:

$$\left. \frac{dN}{d\vec{p}} \right|_{E=E_n} = |\tilde{\psi}_n(\vec{p})|^2, \quad (8)$$

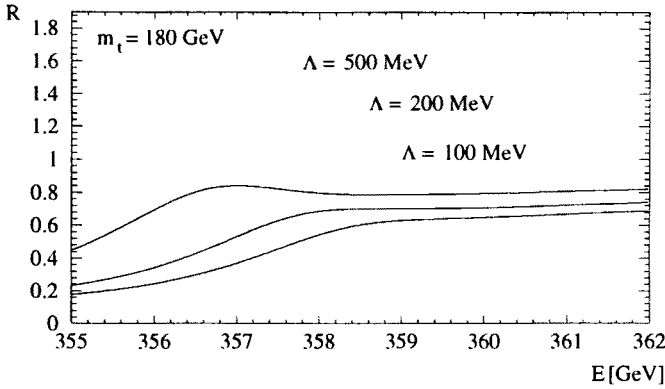


Fig. 6. Production cross section in the threshold region without initial state correction for different values of $\Lambda_{\overline{MS}}$.

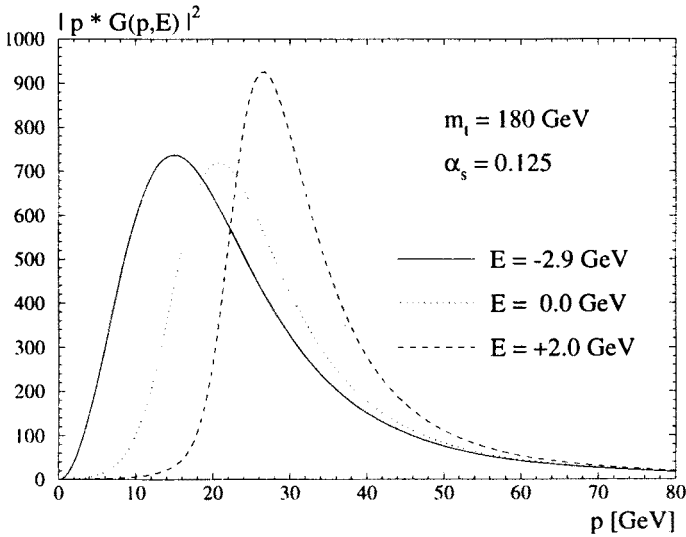


Fig. 7. Green's function $|pG(p, E + i\Gamma_t)|^2$ for $m_t = 180$ and $E = -2.9$ GeV (1s peak) — solid, $E = 0$ — dotted, and $E = 2$ GeV — dashed line.

giving rise to the following differential cross section for a single resonance

$$\frac{d\sigma_n}{d\vec{p}}(\vec{p}, E) = \frac{24\pi^2\alpha^2 Q_t^2}{sm_t^2} |\psi_n(\vec{r}=0)|^2 \frac{\Gamma_t}{(E - E_n)^2 + \Gamma_t^2} |\tilde{\psi}_n(\vec{p})|^2. \quad (9)$$

For a series of overlapping resonances, the momentum distribution of top quarks and the decay products is again conveniently evaluated with the help

of Green's functions [31–33]:

$$\frac{d\sigma}{d\vec{p}}(\vec{p}, E) = \frac{3\alpha^2 Q_t^2}{\pi s m_t^2} \Gamma_t |\mathcal{G}(\vec{p}, E + i\Gamma_t)|^2. \quad (10)$$

$G(\vec{p}, E = i\Gamma)$ can be calculated numerically for complex energies and an arbitrary QCD potential by solving the Lippmann-Schwinger equation

$$\mathcal{G}(\vec{p}, E + i\Gamma_t) = \mathcal{G}_0(\vec{p}, E + i\Gamma_t) + \mathcal{G}_0(\vec{p}, E + i\Gamma_t) \int \frac{d\vec{q}}{(2\pi)^3} \tilde{V}(\vec{p} - \vec{q}) \mathcal{G}(\vec{q}, E + i\Gamma_t), \quad (11)$$

where $\tilde{V}(\vec{p})$ is the potential in momentum space. The free Hamiltonian that is used to define the Green's function \mathcal{G}_0 includes the width. Hence, for the $t - \bar{t}$ system

$$\mathcal{G}_0(\vec{p}, E + i\Gamma_t) = \frac{1}{E - \frac{p^2}{m_t} + i\Gamma_t}. \quad (12)$$

The resulting momentum distribution is shown in Fig. 7 for a characteristic set of energies.

3.4. The potential

At this point a brief discussion is in order on the relation between the top masses determined on the basis of different potentials. The perturbative two loop QCD potential has been calculated in momentum space and is fixed unambiguously for sufficiently large Q^2 :

$$V(Q^2, \alpha_{\overline{MS}}(Q^2)) = -\frac{16\pi}{3} \frac{\alpha_{\overline{MS}}(Q^2)}{Q^2} \left[1 + \left(\frac{31}{3} - \frac{10}{9} n_f \right) \frac{\alpha_{\overline{MS}}(Q^2)}{4\pi} \right] \quad (13)$$

with

$$\frac{\alpha_{\overline{MS}}(Q^2)}{4\pi} = \frac{1}{b_0 \log(Q^2/\Lambda_{\overline{MS}}^2)} \left[1 - \frac{b_1}{b_0^2} \frac{\log \log(Q^2/\Lambda_{\overline{MS}}^2)}{\log(Q^2/\Lambda_{\overline{MS}}^2)} \right],$$

$$b_0 = 11 - \frac{2}{3} n_f, \quad b_1 = 102 - \frac{38}{3} n_f. \quad (14)$$

Power law suppressed terms cannot be calculated in this approach. To evaluate the Fourier transform of this function in order to calculate the potential in coordinate space the small Q^2 behavior has to be specified in an ad hoc manner. Different assumptions will lead to the same short distance behavior. The potentials will, however, differ with respect to their

long distance behavior. In [28] it has been argued convincingly that the long distance tail is cut off by the large top width. However, an additive constant in coordinate space can be induced by the small momentum part of $\tilde{V}(Q^2)$. This additional term would lead to a shift in the $t\bar{t}$ threshold, which in turn can be reabsorbed by a corresponding shift in m_t . These different assumptions are reflected in differences between the predictions of [29, 32, 31] for the precise location of the $t\bar{t}$ threshold for identical values of α_s and m_t and in differences in the α_s dependence of the momentum distributions for fixed m_t and energy. All these differences can be attributed to the freedom in the additive constant discussed before. The same additive constant appears in $b\bar{b}$ spectroscopy, such that the mass difference between top and bottom is independent from these considerations.

3.5. Relativistic corrections

It has been argued in [31, 33] and demonstrated rigorously in [34] that $\mathcal{O}(\alpha_s)$ corrections to the total cross section are absent.

In second order one anticipates effects from relativistic corrections, from the reduction of the phase space through the binding energy and from the Coulomb wave function of the b quark. Individually these effects are large. For the sake of argument, let us adopt a pure Coulomb potential and a binding energy of -2.5 GeV. From the virial theorem one derives a potential energy of -5 GeV. The phase space of the quark decaying first is therefore reduced by this same amount. Assuming $m_t = 150$ GeV one would arrive at a reduction of Γ_t by about 10%. A full calculation of all $\mathcal{O}(\alpha_s^2)$ effects is not available at present and one has to resort to models and analogies [31–33]. For example, it has been shown [35] that the decay rate of a muon bound in the field of a nucleus is given by

$$\Gamma = \Gamma_{\text{free}}[1 - 5(Z\alpha)^2][1 + 5(Z\alpha)^2] \left[1 - \frac{(Z\alpha)^2}{2} \right], \quad (15)$$

where the first correction factor originates from the phase space suppression, the second from the Coulomb enhancement, and the third from time dilatation. Thus there is no first order correction to the total rate from rescattering in the nucleus potential, similar to the $t\bar{t}$ case discussed above. The second order contributions evidently compensate to a large extent. In a model calculation where these features are implemented [33] through a momentum dependent width, it is found that the total cross section as well as the momentum distribution are hardly affected. These considerations have recently been confirmed in a more formal approach [36].

4. Polarization near threshold [37]

The calculations of top polarization well above the threshold for $t\bar{t}$ production were published long ago [38]. Recently also the angular distributions of top quarks [39] and their polarization [37] has been investigated in the threshold region which deserves a special study. This polarization is experimentally accessible as a consequence of the strong analyzing power of leptons from top decay.

Due to restricted phase space the amplitude is dominantly S wave and the electron and positron polarizations are directly transferred to the top quark. For a quantitative study this simple picture has to be extended and the modifications originating from $S - P$ wave interference should be taken into account. As a consequence of final state interaction between t and \bar{t} , which leads to the familiar QCD potential, the parton model prediction where these terms are simply proportional to $\beta = \sqrt{1 - 4m_t^2/s}$ has to be modified. The interference terms are therefore calculated from numerical solutions of Lippmann-Schwinger equations.

We describe the longitudinal polarization of the e^+e^- system in its center-of-mass frame as a function of the variable

$$\chi = \frac{P_{e^+} - P_{e^-}}{1 - P_{e^+}P_{e^-}}, \quad (16)$$

where P_{e^\pm} denote the polarizations of e^\pm with respect to the directions of e^+ and e^- beams, respectively. A righthanded system of coordinates is defined through the triplet of orthogonal unit vectors: \hat{n}_\perp , \hat{n}_N and \hat{n}_\parallel where \hat{n}_\parallel points in the direction of e^- beam, $\hat{n}_N \sim \vec{p}_{e^-} \times \vec{p}_t$ is normal to the production plane and $\hat{n}_\perp = \hat{n}_N \times \hat{n}_\parallel$. In the absence of phases from final state interaction, which can be induced by higher orders in α_s and will be considered elsewhere, the top quark polarization vector is in the production plane and P_\parallel and P_\perp denote its longitudinal and transverse components. The definition of P_\parallel and P_\perp with respect to the beam direction is convenient for the treatment close to threshold and differs from the definition of [38] where the quantities have been defined with respect to the direction of flight of the top quark. The angle ϑ denotes the angle between e^- and the top quark. In the threshold region the top quark is nonrelativistic (with velocity $\beta = p/m_t \sim \alpha_s$) and the kinetic energy of the $t\bar{t}$ system $E = \sqrt{s} - 2m_t$ is of order $\mathcal{O}(\beta^2)$. As a consequence of the $t\bar{t}$ interaction the top quarks will exhibit a momentum spread (Fermi motion) even for fixed energy E . Also the polarization and the angular distribution will depend on both E and p . Retaining only the terms up to $\mathcal{O}(\beta)$ one derives the following expressions for the components of the polarization vector, as functions of E , p and ϑ

$$\mathcal{P}_\parallel(p, E, \vartheta) = C_\parallel^0(\chi) + C_\parallel^1(\chi)\varphi(p, E) \cos \vartheta, \quad (17)$$

$$\mathcal{P}_\perp(p, E, \vartheta) = C_\perp(\chi) \varphi(p, E) \sin \vartheta \quad (18)$$

and, after the integration over top quark momentum p ,

$$P_\parallel(E, \vartheta) = C_\parallel^0(\chi) + C_\parallel^1(\chi) \Phi(E) \cos \vartheta, \quad (19)$$

$$P_\perp(E, \vartheta) = C_\perp(\chi) \Phi(E) \sin \vartheta. \quad (20)$$

The coefficients $C_\parallel^0(\chi)$, $C_\parallel^1(\chi)$ and $C_\perp(\chi)$ are given in [37]. They depend on the polarization χ , the electroweak coupling constants, the Z mass and the center-of-mass energy $\sqrt{s} \approx 2m_t$. They are plotted in Fig. 8 for $m_t = 174$ GeV, $\sin^2 \theta_W = 0.2317$ and $M_Z = 91.1888$ GeV. $C_\parallel^0(\chi)$ and $C_\parallel^1(\chi)$ are shown in Fig. 8(a) as the solid and the dashed lines, respectively, and $C_\perp(\chi)$ as the solid line in Fig. 8(b).

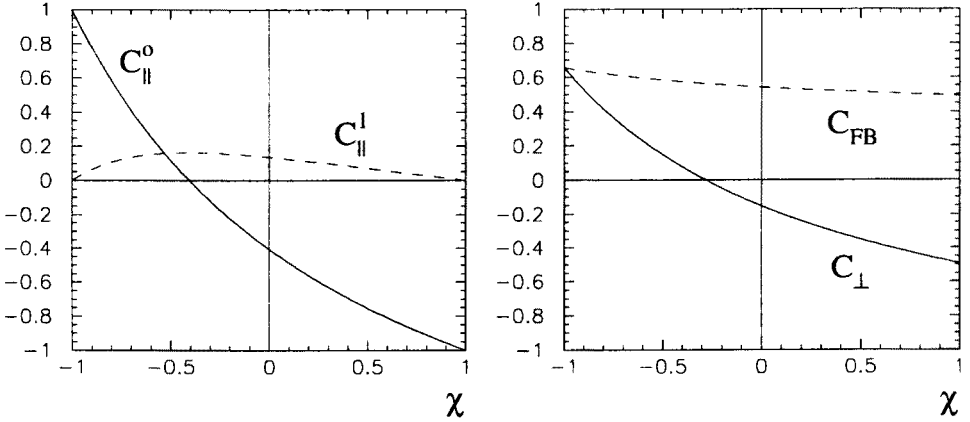


Fig. 8. Coefficient functions: (a) $C_\parallel^0(\chi)$ — solid line and $C_\parallel^1(\chi)$ — dashed line, (b) $C_\perp(\chi)$ — solid line and $C_{FB}(\chi)$ — dashed line.

The functions $\varphi(p, E)$ and $\Phi(E)$ in Eqs (17)–(20) replace the simple factor β in a calculation for free, noninteracting quarks. They describe the complicated dynamics of the $t\bar{t}$ system near threshold which in particular includes effects of the would-be toponium resonances and Coulomb enhancement. Nevertheless, it is possible to calculate these functions using the Green function method. The same functions $\varphi(p, E)$ and $\Phi(E)$ also govern the forward backward asymmetry

$$A_{FB}(E) = C_{FB}(\chi) \Phi(E) \quad (21)$$

which has been first obtained in [39] for $\chi = 0$.

To evaluate the functions $\varphi(p, E)$ and $\Phi(E)$ the Green function method is adequate which has become a standard tool for studying e^+e^- annihilation in the threshold region [28, 29, 32, 31]. In [37] the momentum space approach has been adopted. The Lippmann-Schwinger equation was solved numerically for the S -wave and P -wave Green functions

$$G(p, E) = G_0(p, E) + G_0(p, E) \int \frac{d^3 q}{(2\pi)^3} \tilde{V}(|\vec{p} - \vec{q}|) G(q, E), \quad (22)$$

$$F(p, E) = G_0(p, E) + G_0(p, E) \int \frac{d^3 q}{(2\pi)^3} \frac{\vec{p} \cdot \vec{q}}{p^2} \tilde{V}(|\vec{p} - \vec{q}|) F(q, E), \quad (23)$$

where again

$$G_0(p, E) = \left(E - \frac{p^2}{m_t} + i\Gamma_t \right)^{-1}. \quad (24)$$

In the nonrelativistic approximation the momentum distribution of the top quark is dominated by the S -wave contribution and it is proportional to

$$\mathcal{D}_{S-S}(p, E) = p^2 |G|^2. \quad (25)$$

Contributions of $\mathcal{O}(\beta)$ to \mathcal{P}_{\parallel} and \mathcal{P}_{\perp} as well as to the forward-backward asymmetry \mathcal{A}_{FB} arise from the interference of S - and P -waves and are therefore proportional to

$$\mathcal{D}_{S-P}(p, E) = \frac{p^3 \operatorname{Re}(G F^*)}{m_t}. \quad (26)$$

This distribution exhibits a significantly wider spread in momentum, a feature naturally explained by the larger momentum of P -states. The angular distribution, the forward-backward asymmetry, and the components (17) and (18) of the polarization vector for fixed E and p are then governed by the ratio

$$\varphi(p, E) = \frac{\left(1 - \frac{4\alpha_s}{3\pi}\right) \mathcal{D}_{S-P}(p, E)}{\left(1 - \frac{8\alpha_s}{3\pi}\right) \mathcal{D}_{S-S}(p, E)}. \quad (27)$$

The factors $\left(1 - \frac{4\alpha_s}{3\pi}\right)$ and $\left(1 - \frac{8\alpha_s}{3\pi}\right)$ originate from transversal gluon exchange [40]. In a similar way the function

$$\Phi(E) = \frac{\left(1 - \frac{4\alpha_s}{3\pi}\right) \int_0^{p_m} dp \mathcal{D}_{S-P}(p, E)}{\left(1 - \frac{8\alpha_s}{3\pi}\right) \int_0^{p_m} dp \mathcal{D}_{S-S}(p, E)}, \quad (28)$$

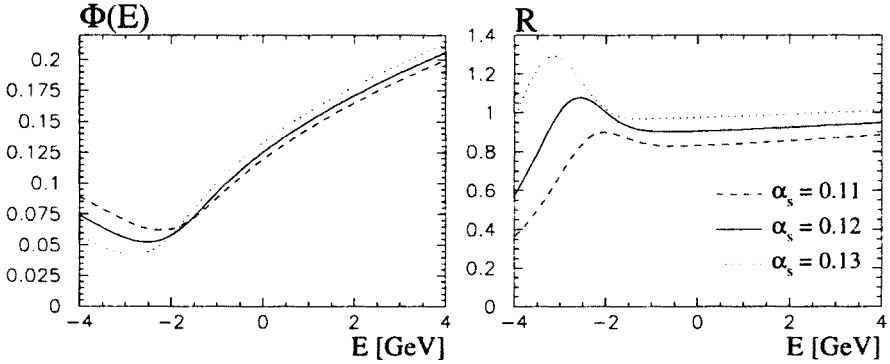


Fig. 9. Energy dependence in the threshold region of: (a) $\Phi(E)$ and (b) $R = \sigma(e^+e^- \rightarrow t\bar{t})/\sigma(e^+e^- \rightarrow \mu^+\mu^-)$ for $m_t = 174$ GeV and $\alpha_s(m_Z) = 0.11, 0.12$ and 0.13 — dashed, solid and dotted lines, respectively.

describes the integrated quantities. The upper limit p_m has been introduced in order to cut off the logarithmic divergence of the numerator. In experimental analyzes the contributions of very large intrinsic momenta will be automatically suppressed by the separation of $t\bar{t}$ events from the background. In [37] $p_m = m_t/3$ was adopted.

The function $\Phi(E)$ is plotted in Fig. 9(a) for $m_t = 174$ GeV. For a comparison in Fig. 9(b) the annihilation cross section $\sigma(e^+e^- \rightarrow t\bar{t})$ is shown in units of $\sigma(e^+e^- \rightarrow \mu^+\mu^-)$. The increase of $\Phi(E)$ with E resembles qualitatively the behavior $\beta \approx \sqrt{E/m_t}$ expected for noninteracting quarks. Linear terms in β amount to typically 0.1 and could, therefore, be accessible experimentally, whereas relativistic corrections $\sim \beta^2$ are evidently small. Combining Figs (8)–(9) the predictions for the polarizations and the angular distributions can be discussed easily. The coefficient $C_{\parallel}^0(\chi)$ governs the leading term for the longitudinal polarization. For $\chi = \pm 1$ the top quark polarization is simply given by the polarization of the incoming electrons, resulting in $C_{\parallel}^0(\chi) = \mp 1$ and $C_{\parallel}^1(\chi) = 0$, and consequently in a nearly completely polarized sample of top quarks, a strong argument for top production with polarized beams. The deviation from the $\beta = 0$ prediction for the longitudinal top polarization is maximal at $\chi \approx -0.4$, where $C_{\parallel}^0(\chi)$ happens to vanish, but remains generally small. The coefficient $C_{\perp}(\chi)$ is small for unpolarized beams. For $\chi = -1$ however, it amounts to 0.65 which leads to sizable polarization of top quarks perpendicular to the beam, if they are produced at large angles. Since leptons from top decays determine its spin with maximal analyzing power, these polarizations may well be measured at a future linear collider.

The contributions of A. Czarnecki, R. Harlander and T. Teubner to the TOPics presented in this review are gratefully acknowledged. Special thanks, however, go to Marek Jeżabek for a long lasting and fruitful collaboration. Without the T_EXnical help of R. Harlander the work would not have been finished in time. I would like to thank the organizers of the Cracow Epiphany Conference on *Heavy Quarks* for the preparation of a pleasant and inspiring workshop. And, mostly important: Happy birthday to Kacper Zalewski and best wishes for a long continuation of his scientific enthusiasm and success.

REFERENCES

- [1] CDF Collaboration, F. Abe *et al.*, *Phys. Rev.* **D50**, 2966 (1994).
- [2] CDF Collaboration, F. Abe *et al.*, preprint FERMILAB-PUB-95/022-E.
- [3] DØ Collaboration, S. Abachi *et al.*, preprint FERMILAB-PUB95/028-E.
- [4] M. Veltman, *Act. Phys. Pol.* **B 8**, 1977 (475).
- [5] D. Schaile, CERN-PPE/94-162.
- [6] J.H. Kühn, *Act. Phys. Pol.* **B 12**, 1981 (347); *Act. Phys. Austr. Suppl.* **XXIV**, 203 (1982); I. Bigi, Y.L. Dokshitzer, V.A. Khoze, J. Kühn, P. Zerwas, *Phys. Lett.* **B181**, 157 (1986).
- [7] M. Jeżabek, J.H. Kühn, *Nucl. Phys.* **B314**, 1 (1989).
- [8] M. Jeżabek, J.H. Kühn, *Phys. Rev.* **D48**, 1910 (1993); Erratum *Phys. Rev.* **D49**, 4970 (1994).
- [9] B.H. Smith, M.B. Voloshin, *Phys. Lett.* **B340**, 176 (1994).
- [10] B.A. Irwin, B. Margolis, H.D. Trottier, *Phys. Lett.* **B256**, 533 (1991).
- [11] A. Denner, T. Sack, *Nucl. Phys.* **B358**, 46 (1991).
- [12] G. Eilam, R.R. Mendel, R. Migneron, A. Soni, *Phys. Rev. Lett.* **66** 1991 (3105).
- [13] A. Denner, A.H. Hoang *Nucl. Phys.* **B397**, 483 (1993).
- [14] F. Borzumati, Proceedings of the Workshop on e^+e^- Colliders at 500 GeV, DESY93-099, pp 261-268.
- [15] G. Eilam, J.L. Hewett, A. Soni, *Phys. Rev.* **D44**, 1473 (1991).
- [16] M. Jeżabek, J.H. Kühn, *Nucl. Phys.* **B320**, 20 (1989); A. Czarnecki, M. Jeżabek, J.H. Kühn, *Nucl. Phys.* **B351**, 70 (1991).
- [17] M. Jeżabek, J.H. Kühn, *Phys. Lett.* **B239**, 317 (1994).
- [18] A. Czarnecki, M. Jeżabek, J.H. Kühn, *Act. Phys. Pol.* **B 20**, 1989 (961); (E) **B23**, 173 (1992).
- [19] M. Jeżabek, C. Jünger, *Act. Phys. Pol.* **B 24**, 1993 (1923).
- [20] B. Grzadkowski, P. Krawczyk, J.H. Kühn, R.G. Stuart, *Nucl. Phys.* **B281**, 187 (1987).
- [21] W. Beenakker, S.C. van der Marck, W. Hollik, *Nucl. Phys.* **B365**, 24 (1991).
- [22] M. Jeżabek, J.H. Kühn, *Phys. Lett.* **B316**, 360 (1993).
- [23] P. Igo-Kemenes *et al.*, DESY 92-123A (1992), Vol. I, p.327.
- [24] T. Sjöstrand, P.M. Zerwas, CERN-TH-6313-91.

- [25] G. Jikia, *Phys. Lett.* **B257**, 196 (1991); V.A. Khoze, W.J. Stirling, Lynne H. Orr, *Nucl. Phys.* **B378**, 413 (1992).
- [26] A. Djouadi, J. Kalinoswki, P.M. Zerwas, *Z. Phys.* **C 54**, 255 (1992).
- [27] K. Hagiwara, H. Murayama, T. Watanabe, *Nucl. Phys.* **B367**, 257 (1991).
- [28] V.S. Fadin, V.A. Khoze, *JETP Lett.* **46**, 525 (1987); *Sov. J. Nucl. Phys.* **48**, 309 (1988).
- [29] J.M. Strassler, M.E. Peskin, *Phys. Rev.* **D43**, 1500 (1991).
- [30] S. Güsken, J.H. Kühn, P.M. Zerwas, *Phys. Lett.* **B155**, 185 (1985).
- [31] M. Jezabek, J.H. Kühn, T. Teubner, *Z. Phys.* **C 56**, 653 (1992).
- [32] Y. Sumino, K. Fujii, K. Hagiwara, H. Murayama, C.-K. Ng, *Phys. Rev.* **D47**, 56 (1993).
- [33] M. Jezabek, T. Teubner, *Z. Phys.* **C 59**, 669 (1993).
- [34] K. Melnikov, O. Yakovlev, *Phys. Lett.* **B324**, 217 (1994).
- [35] H. Überall, *Phys. Rev.* **119**, 365 (1960); R.W. Huff, *Ann. Phys.* **16**, 288 (1961).
- [36] W. Mödritsch, W. Kummer, *Nucl. Phys.* **B430**, 3 (1994).
- [37] R. Harlander, M. Jezabek, J.H. Kühn, T. Teubner, *Phys. Lett.* **B346**, 137 (1995).
- [38] J.H. Kühn, A. Reiter, P.M. Zerwas, *Nucl. Phys.* **B272**, 560 (1986).
- [39] H. Murayama, Y. Sumino, *Phys. Rev.* **D47**, 82 (1992).
- [40] J.H. Kühn, P.M. Zerwas, *Phys. Reports* **167**, 321 (1988).